THE JOURNAL OF PHYSICAL CHEMISTRY C
A JOURNAL OF THE AMERICAN CHEMICAL SOCIETY

pubs.acs.org/JPCC

Article

Role of Oxygen in Vacancy-Induced Phase Formation and Crystallization of Al_2TiO_5-Based Chemical Vapor-Deposited Coatings

Sebastian Öhman, Axel Forslund, Rebecka Lindblad, Gyula Nagy, Peter Broqvist, Elin Berggren, Fredrik O. L. Johansson, Tobias Törndahl, Daniel Primetzhofer, and Mats Boman*

Cite This: *J. Phys. Chem. C* 2023, 127, 6456−6465

Read Online

ACCESS | Metrics & More | Article Recommendations | Supporting Information

ABSTRACT: Oxygen is a commonly overlooked element influencing the properties of many metal oxides. By combining several analytical *in situ* techniques and theoretical calculations, we demonstrate that oxygen plays a vital part in the phase formation and crystallization of Al_2TiO_5-based chemical vapor-deposited coatings. Rutherford backscattering spectrometry (RBS) corroborates a polymorphic transformation during crystallization. Subsequent hard X-ray photoelectron spectroscopy (HAXPES) shows that crystallization occurs through a displacive (diffusionless) mechanism. Coupled with theoretical calculations, the crystallization and co-formation of Al_2TiO_5, $Al_6Ti_2O_{13}$, and $Al_{16}Ti_5O_{34}$ are suggested to be driven by the migration of oxygen ions and their corresponding vacancies.

INTRODUCTION

Conventional synthesis routes strongly rely on diffusion as a rate-limiting step,[1] which impedes the ability to target many promising multicomponent and metastable phases.[2] These phases may carry superior properties compared to their stable counterparts,[3] making them attractive for use in many contemporary and emerging technologies.[4] In particular, this concerns the development of various metal oxides,[5] showing a wide range of different properties depending not solely on their chemical compositions and stoichiometries but also on their local short-range features.[6,7] The ability to adapt, control, and modify these features hinges on the close interplay between the synthesis conditions and the various reaction pathways that are conceivable from the synthesis.[8,9] But when diffusion governs the process, few options are available to effectively reduce the energy barriers, steer the reaction coordinates, and achieve predictable reaction kinetics toward the most desirable products.[10,11] In addition, computational methods frequently assume diffusion as the governing process when predicting the possible phase outcomes from a given material system.[12] While these approaches provide a thermodynamic map of the accessible phase landscape, scarce information is given on the best way to reach them kinetically.[13] The lack of a synthesis framework that may encompass both of these parts represents an essential and missing cornerstone to achieve functional inorganic materials from rational planning and design.[11,14,15] Bridging this gap would also facilitate the fabrication of new material combinations and phases with extended and unique properties. Therefore, finding and establishing new synthesis methods that rely more on kinetical considerations—rather than thermodynamic ones—remains of fundamental importance to the field of inorganic chemistry.[2,9−11,16]

In this respect, the crystallization of amorphous intermediates offers an attractive way to circumvent typical diffusional constraints and allows enhanced kinetic control of the synthesis. Such routes include, for instance, the fabrication of amorphous layers using soft-chemistry-based and thin-film deposition techniques. Novet and Johnson pioneered this strategy in the early nineties, showing how conventional limitations of diffusion-based solid-state reactions could be overcome by allowing nucleation—a kinetic phenomenon—to control the synthesis.[16] A good elemental homogeneity and a short-range ordering within the amorphous layers are essential to achieve this.[17] In those scenarios, nucleation favors the formation of phases with the lowest nucleation barriers and not necessarily the most thermodynamically stable ones.[16−20] Thus, assuming that the composition of the amorphous layers can be controlled, this route opens opportunities to trap both known and unknown phases through means of kinetic selectivity.

Such kinetic selectivity can be obtained through simultaneous depositions of metal−organic precursors.[21] Specifically, this is realized from chemical vapor deposition (CVD), which entails a good mixing of the precursors in the gaseous state, allowing for an equally good mixing of elements in the growing coating. Combined with targetable kinetics, this also favors the formation of heterometallic M−O−M* bond assemblages, a

Received: December 7, 2022
Revised: March 16, 2023
Published: March 27, 2023

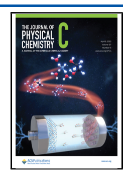

https://doi.org/10.1021/acs.jpcc.2c08570
J. Phys. Chem. C 2023, 127, 6456−6465

reaction step that otherwise is typically associated with steep energy barriers when diffusion controls this process.[22] Accordingly, synthesizing amorphous coatings with good elemental homogeneity by CVD, followed by a subsequent nucleation-controlled crystallization step, allow for new possibilities to make multicomponent oxides at reduced temperatures, shorter timescales, and with better yields than comparable (conventional) techniques.

Recently, we have demonstrated this route in fabricating aluminum titanate-based (Al_2TiO_5) coatings.[21,23] Al_2TiO_5 is a refractory ceramic that is challenging to make from conventional diffusional-based techniques. The properties of this material include, among many, a low-to-negative thermal expansion,[24,25] high thermal shock resistance,[26] good corrosion resistance,[27,28] and a self-healing of cracks at elevated temperatures.[29,30] These properties make the phase a potential candidate for many high-temperature and metallurgical applications.[31] Besides Al_2TiO_5, we have also encountered some unconventional phases in the Al−Ti−O system by this synthesis route, such as $Al_6Ti_2O_{13}$ and $Al_{16}Ti_5O_{34}$. These phases are structurally similar to Al_2TiO_5, with the main differences being their different stacking sequences along their *c*-axes which, in turn, are caused by the presence of lower-coordinating sites.[32−35] However, the mechanism and synthesis conditions controlling these phases' formation and material characteristics remain mostly unknown.

Likewise, few syntheses can be proclaimed to be nucleation-controlled,[14] especially since most crystallization processes are so closely linked with diffusion.[36] Although the physical factors promoting nucleation are relatively understood, not least by the framework comprising classical nucleation theory (CNT), the fundamental mechanisms influencing its origin, development, and duration are less so. Understanding these mechanisms would contribute to achieving complete kinetic control of the phase evolutions by nucleation. Also, this may enable new intriguing ways to adapt the crystallizing media's microstructural development and subsequent properties.

Nevertheless, reaching such a profound understanding of nucleation is challenging by most experimental (empirical) means, particularly when considering that nucleation is a dynamic process occurring in very short time and length scales. Hence, *in situ* techniques are typically required to evaluate these events thoroughly. While our previous examinations of the crystallization kinetics have focused on the elemental influence of the cations,[23] the role of oxygen remains to be clarified during the crystallization of Al_2TiO_5, $Al_6Ti_2O_{13}$, and $Al_{16}Ti_5O_{34}$.

Therefore, in this study, we bring new understandings to the role of oxygen during the crystallization and phase evolution of the Al−Ti−O system by combining several *in situ* analytical techniques and theoretical calculations based on density functional theory (DFT). Specifically, Rutherford backscattering spectrometry (RBS), providing essential information about the development of the chemical composition during crystallization, is used together with hard X-ray photoelectron spectroscopy (HAXPES), providing in-depth information about the bonding characteristics. Combined, these techniques enable us to unravel the mechanisms leading to the formation and crystallization of Al_2TiO_5, $Al_6Ti_2O_{13}$, and $Al_{16}Ti_5O_{34}$.

The role of oxygen has previously been shown to have a peculiar influence on crystalline Al_2TiO_5's thermal stability at elevated temperatures. For instance, it has been demonstrated that the partial pressure of oxygen affects the phase's stability and subsequent decomposition into its two binary constituents,[37,38] being frequently reported as TiO_2 (rutile) and α-Al_2O_3,[39] especially in oxygen-rich environments.[40] However, in oxygen-deficient ones, Al_2TiO_5 has been suggested to decompose into Ti^{3+}-containing compounds, including sub-oxide compounds like Ti_3O_5, Ti_2O_3 (tistarite), and so-called Magnéli phases (Ti_nO_{2n-1}).[37,41] These studies collectively illustrate that oxygen's role can significantly affect the structural integrity and stability of the Al_2TiO_5 phase. Notably, the limited thermal stability of Al_2TiO_5 at intermediate temperatures (*e.g.*, 800−1300 °C)[38,42] currently hampers the phase's practical applicability, thus creating incentives to improve its thermal stability further.

■ METHODS

Deposition Process. As-deposited (amorphous) Al_2TiO_5-based coatings were prepared on p-type Si 100 substrates through simultaneous depositions of titanium isopropoxide and aluminum isopropoxide in an in-house-built CVD instrument. Depositions were made at 450 °C for 1 h. Detailed experimental and technical descriptions of the CVD process can be found elsewhere.[21]

RBS/EBS In Situ Measurements. Rutherford/Elastic backscattering spectrometry measurements were carried out in the SIGMA chamber, employing the 5 MV pelletron tandem accelerator at Uppsala University. SIGMA is equipped with an electron-beam heater, allowing for *in situ* annealing of the samples. The annealing temperature is accurately monitored from outside of the chamber using an infrared thermometer (Optris CT laser). For the RBS/EBS measurements, a beam of He^+ ions with 3.037, 3.137, and 3.237 MeV primary energy was used. This way, the narrow $^{16}O(\alpha,\alpha 0)^{16}O$ resonance at 3.037 MeV could be exploited to sensitively probe the O content on and approximately 0.5−1 μm below the surface. All energies were measured before and after annealing at 800 °C for 1 h. The tilt angle of the sample normal was 5° with respect to the incident beam direction, while the scattering angle was 170°. RBS/EBS spectra were fitted by the SIMNRA code, version 7.02.[43] A detailed description of the tandem laboratory at Uppsala University can be found elsewhere.[44]

Theoretical Calculations. The DFT calculations of the antisite defect exchange energies and oxygen ion migrations were calculated within the projector augmented wave (PAW) method as implemented in the VASP software.[45−49] The Perdew−Burke−Ernzerhof (PBE) functional[50] was used for the exchange−correlation energy. For the integration over the Brillouin zone, a mesh[51] corresponding to at least 2000 kp/atom^{-1} was used with the Methfessel−Paxton method.[52] A 500 eV energy cutoff was used.

To simulate the migration paths of oxygen and its corresponding vacancies, the nudged elastic band (NEB) method was used.[53] During the NEB calculations, five images were used at constant volume. The minimum energy path was considered to be converged when the maximal force on the unconstrained atoms was less than 0.05 eV/Å. All oxygen vacancies and NEB calculations were performed using the Atomic Simulation Environment (ASE).[54]

HAXPES Measurements. Hard X-ray photoelectron spectroscopic measurements were carried out at the Soleil synchrotron radiation facility, Paris, using the HAXPES end station of the Galaxies beamline at the in-vacuum U20 undulator source. The instrument was equipped with a Scienta EW4000 spectrometer. Photon energy of 8000 eV was selected

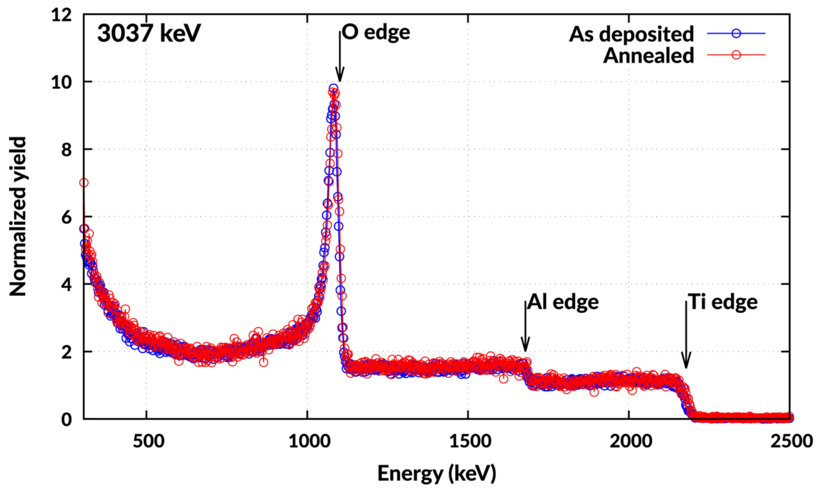

Figure 1. EBS spectra acquired using an incident beam of 3037 keV He^+ for as-deposited and annealed samples with close-to-ideal stoichiometry. Additional spectra using different incident beam energies are provided in the Supporting Information.

using a double-crystal monochromator. This energy was used for all measurements. Samples were mounted on top of tantalum sample plates (Omicron flag style) and spot welded onto the plates using tantalum foil strips. Sample charging was mitigated using a Coscon FG flood gun (SPECS GmbH) operating at 150 V energy and 500 μA emission. Survey scans were recorded with- and without charge compensation in the binding energy (BE) range 900−0 eV, using 250 meV step- and 500 eV pass energies. Detailed core-level spectra were collected for Ti 2p (BE 510−445 eV); Al 2s (BE 130−105 eV); O 1s (BE 560−520 eV); C 1s (295−278 eV); Ti 1s (BE 5003−4950 eV); Al 1s (1571−1554 eV); and also the valence band (40−0 eV). A step of 100 meV and a pass energy of 100 eV was used when collecting these spectra. The binding energy scale was calibrated by placing the valence band edge of the survey spectrum at 0 eV and then using the core-level position as the reference for the detailed core-level spectra. Measurements were made before and after annealing *in situ* for 3 h at 800 °C. The annealing was performed within the preparation chamber, using a tungsten filament wire located on the manipulator behind the sample plate. During annealing, the sample surface temperature was monitored using a pyrometer with an emissivity (ε) setting to 0.8. The heating rate was approximately 30 °C/min.

■ RESULTS AND DISCUSSION

Classical nucleation theory (CNT) assumes that the emerging nuclei and the final crystallized phase share similar macroscopic properties (*i.e.*, density, structure, composition).[55,56] Therefore, given a uniform (homogeneous) chemical composition of our amorphous coatings, a single crystalline phase should be expected to arise during the phase transition; namely, the phase whose stoichiometry is closest to the overall composition of the amorphous layer.[20,57] Nonetheless, previous examinations have revealed that a significant co-formation of $Al_6Ti_2O_{13}$ and $Al_{16}Ti_5O_{34}$ also happens even when the Al−Ti ratio in the coating is close-to-ideal (1.93) with respect to the Al_2TiO_5's stoichiometry (*i.e.*, 2−1).[21,23] This infers a possibility for compositional fluctuations to be the main reason for the co-formation of $Al_6Ti_2O_{13}$ and $Al_{16}Ti_5O_{34}$. Indeed, such compositional variations and elemental enrichments are a typical deviation from CNT and have frequently been reported in the crystallization of many glass-forming materials.[58−60]

In order to investigate the possibility of compositional fluctuations during crystallization, Rutherford/elastic backscattering spectrometry (RBS/EBS, see Methods) was carried out on ∼ideal stoichiometric samples annealed *in situ*. Experiments were performed in the SIGMA chamber[61] of the 5 MV tandem pelletron accelerator, at Uppsala University. We used a primary beam of He^+ ions with 3037, 3137, and 3237 keV incident energies. By this approach, we were able to exploit the 3037 keV O resonance[62] for depth profiling of the oxygen content in the film with high accuracy. Measurements were made before and after annealing at 800 °C, a temperature where the coatings readily crystallize,[21,23] for 1 h. A typical result is shown in Figure 1, and additional spectra can be viewed in the Supporting Information (Figures S1 and S2), essentially showing similar results. Moreover, diffractograms showing the phase formations and crystallinity after annealing are provided in Figures S3 and S4.

As shown in Figure 1, there is no detectable alteration of the spectrum due to the crystallization. This means that substantial compositional fluctuation, such as long-range diffusion, elemental segregation, or loss or gain of oxygen, does not occur as part of the amorphous-to-crystalline phase transition. In essence, the results show that the crystallization process is polymorphic and that compositional effects cannot be responsible for causing the co-formation of the $Al_6Ti_2O_{13}$ and $Al_{16}Ti_5O_{34}$ phases. In particular, this is true within the ∼ideal stoichiometric domain. Furthermore, this conclusion remains valid within the long-range ordering of the crystalline samples, thus strengthening the belief that possible local variations and features in the short-range order are determinants for the formation of the $Al_6Ti_2O_{13}$ and $Al_{16}Ti_5O_{34}$ phases beyond Al_2TiO_5.[21]

Such local variations can be induced by the existence of mixed oxidation states, especially regarding titanium's chemical state. When Hoffmann et al. originally described and synthesized the $Al_6Ti_2O_{13}$ and $Al_{16}Ti_5O_{34}$ phases, they noted that their samples, synthesized by the solid-state route, had a "transparent deep blue to light blue" color.[35] Typically, a blueish tint is a signifying feature of oxygen vacancy-induced Ti^{3+}-ions in substoichiometric titania phases.[63−66] The potential presence of Ti^{3+} during the simultaneous formation

https://doi.org/10.1021/acs.jpcc.2c08570
J. Phys. Chem. C 2023, 127, 6456−6465

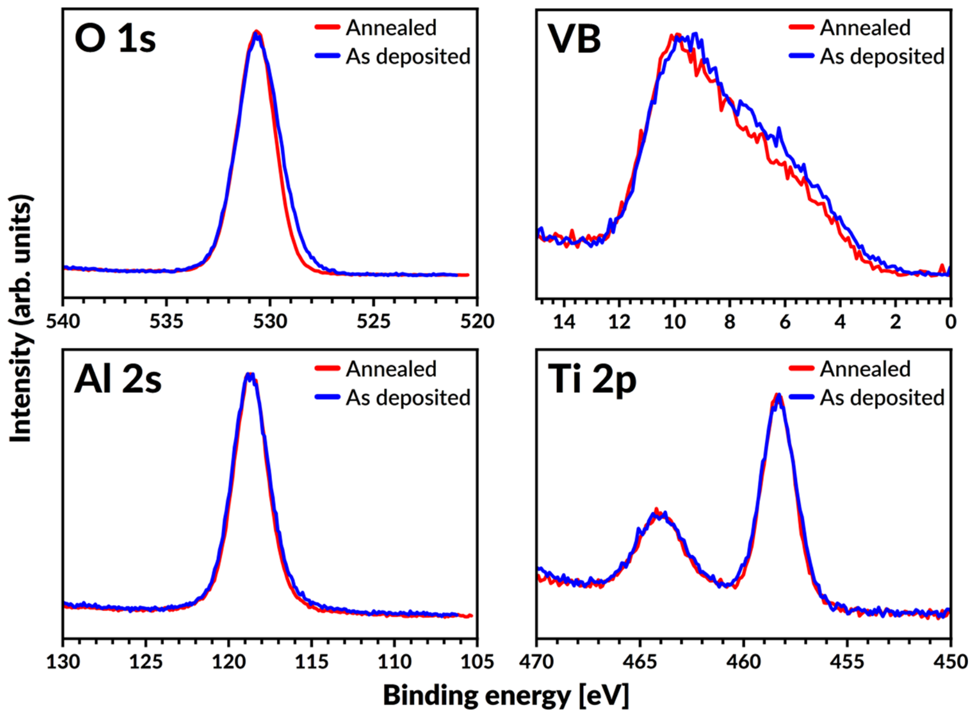

Figure 2. O 1s, Al 2s, Ti 2p core levels along with valence band (VB) measurements before and after annealing at 800 °C, using 8000 eV photon energy.

of these phases would suggest that $Al_6Ti_2O_{13}$ and $Al_{16}Ti_5O_{34}$ are decomposition products to Al_2TiO_5, and possibly also intermediate reaction states to any stable binary constituents, like Al_2O_3 or TiO_2. Also, it implies that the crystallization and possible thermal decomposition of Al_2TiO_5 at lower temperatures are interchangeable—rather than separate—processes. Therefore, it is vital to elucidate the potential presence of different oxidation states as part of the crystallization event.

Previous X-ray photoelectron spectroscopy (XPS) examinations by Innocenzi et al. on sol−gel synthesized $Al_xTi_yO_z$ coatings have shown that Al^{3+} and Ti^{4+} were the sole entities in the samples after annealing.[67] However, XPS is a highly surface-sensitive technique, and it is still possible that the oxidation states of titanium differ between the bulk and the topmost layer of the coating. In this sense, HAXPES can probe deeper into the coating, hence providing essential information about the chemical states in the bulk of the sample.[68]

For these reasons, we carried out a set of HAXPES measurements on ∼ideal stoichiometric samples before and after annealing, which was made *in situ* using the HAXPES end station of the GALAXIES beamline at synchrotron Soleil, Saint-Aubin, Paris.[69,70] Evaluations of the main core-level spectral features corresponding to O 1s, Al 2s, Ti 2p, and the valence band (VB), using 8000 eV photon energy, are presented in Figure 2. Additional core-level spectra (C 1s, Al 1s, and Ti 1s) are further provided in the Supporting Information, Figures S5 and S6, along with survey scans in Figure S7. As a general comment on the purity of the coatings, a small residual C 1s signal remains after annealing, which we ascribe to potentially trapped residues from the deposition process. That said, additional measurement by time-of-flight elastic-recoil detection analyses (ToF-ERDA), being highly sensitive to lighter elements, confirms that the coating's overall carbon and hydrogen content after annealing are exceptionally low (*i.e.*, below 1 atom %). The ToF-ERDA results are also provided in the Supporting Information, Figure S8.

Figure 2 indicates no spectral change in the cationic environments due to annealing and crystallization. Essentially, this implies that no significant stoichiometric changes by the cations occur on the local short range due to the crystallization, which agrees with the results from the RBS/EBS measurements. The binding energy values of the measured spectral lines agree with those typically found in the literature, corresponding coherently to the presence of Al−Ti−O-containing oxides.[67,71] However, no straightforward method exists allowing separation of the chemical environments belonging to Al_2TiO_5, $Al_6Ti_2O_{13}$, and $Al_{16}Ti_5O_{34}$ by merely considering the binding energies and peak shapes of these core levels.

The peak positions and shape of the Ti $2p_{3/2}$ level demonstrate the predominant presence of Ti^{4+} specimens in the coating before and after annealing.[72,73] This is also corroborated by the performed peak fitting, shown in Figure S9 in the Supporting Information, where any potential contribution of Ti^{3+} is practically negligible. Since we have previously established the co-formation and crystallization of $Al_6Ti_2O_{13}$ and $Al_{16}Ti_5O_{34}$ in the annealed samples by X-ray diffraction,[21,23] we can conclude that Ti^{3+} is not likely a structural entity belonging to any of these phases. Thus, $Al_6Ti_2O_{13}$ and $Al_{16}Ti_5O_{34}$ are independent phases with unique Al−Ti stoichiometries. Nevertheless, it is essential to clarify that this does not exclude the possibilities of Ti^{3+} formation as part of the thermal decomposition of these phases, which may occur at even higher temperatures and after prolonged annealing durations, especially in oxygen-free environments.

While no changes in chemical environments appear for the cations, a different picture emerges for the anions. Mainly, a subtle shift and sharpening of the O 1s core level, particularly on the low-energy side, is observable upon annealing and crystallization. This is also coupled with a similar behavior displayed by the valence band. Knowing that the valence band contains information about the electrons that partake in the chemical bonding, any changes to this band would indicate structural rearrangements of the local short range. Since the difference is coupled with analogous changes in the oxygen core level, which becomes narrower and thereby represents more ordered bond configurations, we can deduce that short-range displacive changes to oxygen bond configurations are predominantly required for the crystallization of Al_2TiO_5, $Al_6Ti_2O_{13}$, and $Al_{16}Ti_5O_{34}$. In other words, a transition requiring limited diffusion to occur. Notably, this also agrees with our RBS/EBS findings and previous Raman spectroscopic examinations,[21] indicating structural rearrangements and changes to the local coordination during crystallization. Innocenzi et al. also suggested a diffusionless crystallization process of their sol−gel synthesized $Al_xTi_yO_z$ coatings;[67] however, their reasoning was based solely on the high degree of structural homogeneity in the short-range order, not by any structural migrations of oxygen.

By ruling out the possibility of compositional fluctuations and mixed oxidation states during crystallization, a final cause exists that could explain the co-formation of $Al_6Ti_2O_{13}$ and $Al_{16}Ti_5O_{34}$; namely, if a homogeneity region exists that allows these phases to be formed. Interestingly, such a homogeneity region is not commonly displayed in conventionally available thermodynamic Al−Ti−O phase diagrams, where Al_2TiO_5 is solely represented as a single-line phase.[74] However, a homogeneity region can also be induced by structural defects,[75−79] including Schottky, Frenkel, vacancies, and antisite exchange defects. Especially for oxides, a strong relationship may exist between vacancy concentrations and the molar volume of a given compound, resulting in increased chemical expansivities and local lattice variations.[80,81] Although Hoffmann et al. never explored the possibilities of such variations, the presence of stacking faults was suggested to be a key feature found in $Al_{16}Ti_5O_{34}$.[32] Interestingly, such planar defects can be induced through aggregation and clustering of zeroth-order (point) defects, including vacancies.[82]

To explore the presence and role of defect formations in Al_2TiO_5 and $Al_6Ti_2O_{13}$, we begin by carrying out first-principle *ab initio* calculations by density functional theory (DFT) to extract antisite defect exchange energies $\Delta E_{antisite}$ between Al and Ti lattice sites. We regard three arbitrary Al site positions in Al_2TiO_5 and $Al_6Ti_2O_{13}$, here denoted as Al1, Al2, and Al3, to obtain different antisite exchange defect values. The sites can be viewed in Figure 3. In Al_2TiO_5, the sites are octahedrally coordinated to oxygen, whereas in $Al_6Ti_2O_{13}$, the Al3 site has a lower coordination in the form of a trigonal bipyramid,[35] *cf.* Figure 3b.

Formally, $\Delta E_{antisite}$ denotes the energy difference between the lowest energetic configuration where an antisite defect exists compared to the ordered configuration.[83] Hence, we have

$$\Delta E_{antisite} = E_{antisite} - E_{ordered}$$

where $\Delta E_{antisite}$ and $E_{ordered}$ represent the formation energy of the single-disordered and ordered configurations, respectively. The calculated values are given in Table 1 for Al_2TiO_5 and $Al_6Ti_2O_{13}$. Because of the large unit cell of $Al_{16}Ti_5O_{34}$ and the number of atoms it contains, it is difficult to correctly determine this phase's ordered (ground-state) configuration. Notwithstanding this limitation, $Al_{16}Ti_5O_{34}$ is structurally similar to Al_2TiO_5 and $Al_6Ti_2O_{13}$, both on the short- and long-range levels.[32] Therefore, it is reasonable to assume that the values calculated for Al_2TiO_5 and $Al_6Ti_5O_{13}$ also scale towards $Al_{16}Ti_5O_{34}$ in a similar—albeit not necessarily equal—manner.

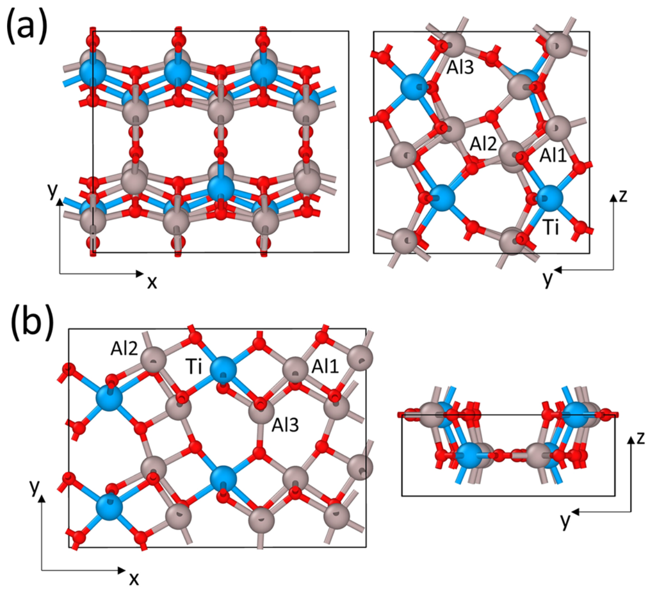

Figure 3. Illustration of the (a) Al_2TiO_5 and (b) $Al_6Ti_2O_{13}$ unit cells with the different sites marked for the antisite defect exchange energies.

Table 1. Calculated Antisite Exchange Defect Energies for the Al_2TiO_5 and $Al_6Ti_2O_{13}$ Phases

	antisite exchange defect energies	
	Al_2TiO_5 (128 atoms)	$Al_6Ti_2O_{13}$ (168 atoms)
Al1 (eV)	0.29	0.09
Al2 (eV)	0.43	0.16
Al3 (eV)	0.47	0.45

By reviewing the values found in Table 1, it is found that the calculated values are positive, meaning that the ordered structure is energetically more stable compared to the disordered ones. The calculated values are small nonetheless, suggesting that they can easily be overcome in a Gibbs free-energy model where contributions from vibrational and configurational entropies are included. For instance, if we assume a simplified mean-field approach,[84] where (1) the defect formation energies are assumed to be independent of the composition, (2) neglect any defect−defect interactions (*i.e.*, clustering), and (3) assume that the $E_{antisite}$ is proportional to the number of defects N_v, we find that a transition temperature (T_{trans}) to obtain cationic disordering is typically below 800 Kelvin. This indicates that antisite defect formations are extensive in Al_2TiO_5 and $Al_6Ti_2O_{13}$, especially at elevated temperatures.

Overall, these results conform with experimental findings employing transmission electron microscopy[85] (TEM) and various diffraction techniques,[24,25,86] showing that Al_2TiO_5, in particular, readily displays cationic mixing. Furthermore, the calculated $E_{antisite}$ values presented herein are in the same range as those originally given by Grimes and Pilling (0.20−0.64 eV), who used a simplified force field model to derive values of antisite energies in Al_2TiO_5.[87]

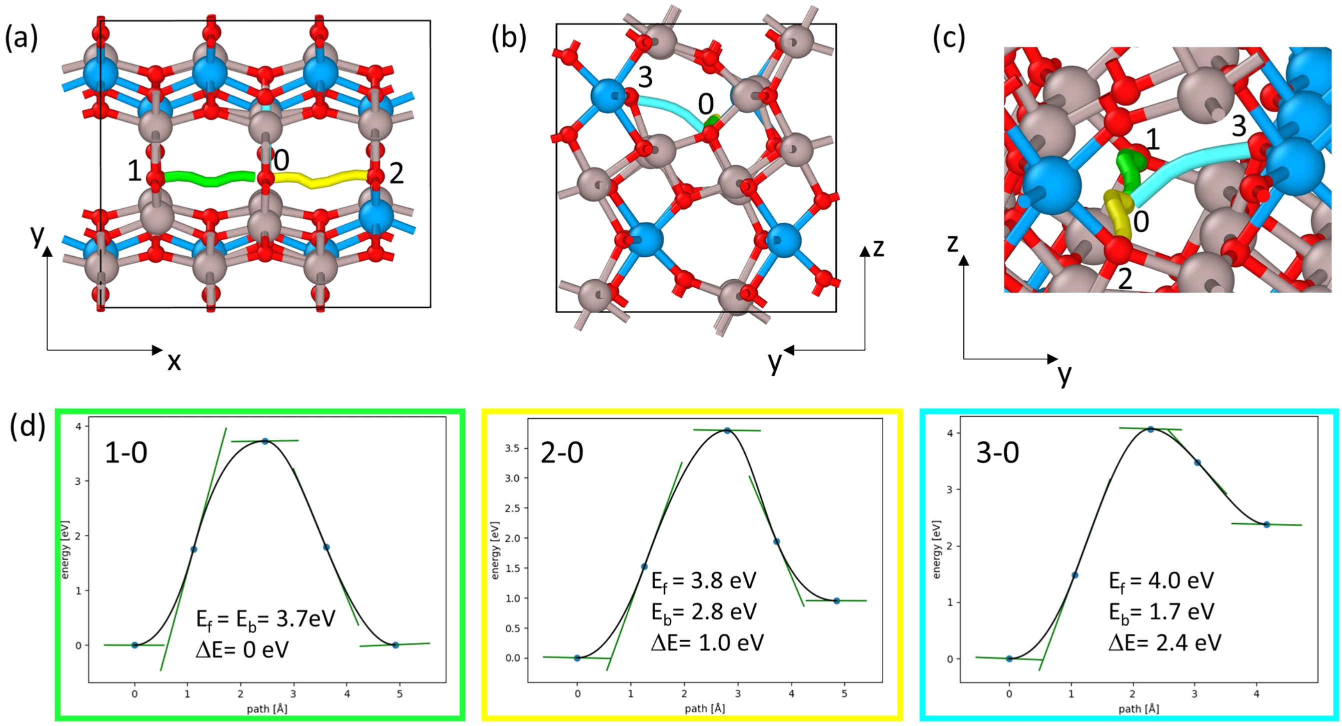

Figure 4. (a−c) Visualization of migration pathways for oxygen in Al_2TiO_5, shown by different cell projections. (d) Different forward (E_f) and backward (E_b) barrier energies corresponding to oxygens movement from positions 1, 2, and 3 to position 0, respectively. Each migration pathway is also listed and described in the text. ΔE denotes the difference in vacancy formation energy between two designated positions.

Two main implications can be drawn from our findings. First, since the calculated $E_{antisite}$ values for $Al_6Ti_2O_{13}$ are in the same range as those calculated for Al_2TiO_5, a significant cationic mixing in $Al_6Ti_2O_{13}$ can also be expected. In addition, the lower-coordinating sites in these phases do not seem to influence the possibilities of antisite defect formation either. Regardless, Hoffmann et al. assumed that the lower-coordinating sites were solely occupied by aluminum in $Al_6Ti_2O_{13}$ and $Al_{16}Ti_5O_{34}$,[32,33] implying that a potential cationic ordering in these phases could still form and exist.

Second, the low and similar antisite defect exchange energies between Al_2TiO_5 and $Al_6Ti_2O_{13}$ (and possibly also $Al_{16}Ti_5O_{34}$), along with their structural resemblances, implicate that no or minimal diffusion should be required to form any of these phases. Notably, this agrees with our RBS and HAXPES results. If significant diffusion is not needed, then structural relaxations should predominantly account for these phases' origin and subsequent crystallization. Given that a short-range ordering of Al−O−Ti bonds already exists in the amorphous coatings,[21] it is reasonable to assume that such relaxations should primarily involve structural displacements and short-range migrations of the oxygen framework. This is also supported by our HAXPES results and strengthened by knowing that Grimes & Pilling have shown high energy barriers to the migration of the cations (6.10−11.30 eV) in Al_2TiO_5 by Schottky and Frenkel formations.[87]

Based on the inferences pointing to the influence of oxygen, we carried out additional theoretical calculations with DFT that solely focused on oxygen's migration and possible vacancy formations in the Al_2TiO_5 structure. The oxygen vacancy models were made charge neutral by replacing two Ti atoms (formally in the +4 oxidation state) with Al atoms (formally in the +3 oxidation state) for every removed O atom. This approach follows our HAXPES results—showing only Ti^{4+} in the annealed samples—and the low energies calculated for antisite Al(Ti) defect formations (*cf.* Table 1).

By using DFT, several different Al_2TiO_5 configurations were evaluated. Among these, one of the low-energy configurations was selected for the oxygen ion migration studies, where the oxygen vacancy is located in a three-coordinated site with only Al^{3+} ions as the nearest neighbors, *cf.* Figure 4. This configuration is possible because the compensating Al^{3+} ions are placed in the same Ti-row (*cf.* Figures 3 and 4). Separating Al^{3+} ions into different Ti rows was found to be of equal stability.

From the selected configuration, we find three possible oxygen ion migration pathways to fill the vacancy, namely:

(1) Oxygen moves from a nearby aluminum-bonded (geometry equivalent) position in the same row (pathway 1−0), thus with no change in coordination number.
(2) Oxygen moves from a nearby position bonded to two aluminum and one titanium ion to the only aluminum-bonded position in the same row (pathway 2−0), again with no change in coordination number.
(3) Oxygen moves from an enclosed position bonded to two aluminum and two titanium ions between rows (pathway 3−0). This movement implies that the oxygen ion reduces its coordination number from 4 to 3.

These migration pathways are visualized in Figure 4a−c, with final energy barriers and energy differences presented in Figure 4d. The energy barrier values are also listed in Table 2 for easier comparison.

As discussed above and seen in Figure 4d, there are large energy penalties associated with oxygen vacancies in the vicinity of Ti^{4+} ions. For example, in the structure shown in Figure 4, the oxygen ion is most stable in position 3, which is a

Table 2. Calculated Minimum Energy Barriers Corresponding to the Migration of Oxygen Ions (and Its Coupled Vacancy Formation) in Al_2TiO_5[a]

migration path (see Figure 4)	E_b (eV)	E_f (eV)	ΔE (eV)
0−1/1−0	3.7	3.7	0
0−2/2−0	2.8	3.8	1.0
0−3/3−0	1.7	4.0	2.4

[a]The migration paths are shown in Figure 4.

four-coordinated site with two Al^{3+} and two Ti^{4+} nearest neighbors. These energy penalties affect the migration of oxygen, making the energy barriers heavily dependent on its migration pathway. While the migration of vacancies into the vicinity of Ti^{4+} ions yields steep barriers around 4 eV (case 1−0, 2−0, and 3−0) in Figure 4d, the barrier for moving the oxygen ion in the opposite direction is consequently significantly smaller. Specifically, moving the vacancy away from the Ti^{4+} ion, expressed by the migration pathways 0−2 and 0−3, yields energy values around 2.8 and 1.7 eV in our calculations, respectively. Interestingly, the latter value is within reach for the typical annealing temperatures where Al_2TiO_5 has been found to crystallize, *i.e.*, 1073 Kelvin. The computed values presented herein can also be regarded to represent upper-bound values for the migration of oxygen and its vacancies as they have been made for the crystalline state of Al_2TiO_5. The migration barriers for oxygen are expected to be lower in the amorphous (disordered) state.

Given that no significant compositional variations occur during crystallization, and that displacive changes to oxygen mainly occur after annealing, these calculations further support that oxygen migration is likely responsible for the transition between the disordered and ordered states in Al_2TiO_5. Since oxygen's migration is coupled with vacancy formations, the calculations further indicate that titanium ions prefer higher oxygen coordination environments in Al_2TiO_5. Likewise, vacancies seem to conglomerate—or possibly even order—around aluminum ions during crystallization, which is in agreement with the structural descriptions of $Al_6Ti_2O_{13}$ and $Al_{16}Ti_5O_{34}$ as previously given by Hoffmann et al.[32,35] Accordingly, our results suggest that the crystallization and co-formation of Al_2TiO_5, $Al_6Ti_2O_{13}$, and $Al_{16}Ti_5O_{34}$ are driven by the migrations of oxygen and its corresponding vacancies.

To summarize, the findings presented in this study coherently emphasize the involvement and role of oxygen in the phase formations and crystallization of Al_2TiO_5, $Al_6Ti_2O_{13}$, and $Al_{16}Ti_5O_{34}$ titanate phases. Potentially, a similar role of oxygen may be found among other family group pseudobrookite and oxide compounds that share similar structural features to these phases.

CONCLUSIONS

The role of oxygen during phase formation and crystallization of coatings containing Al_2TiO_5, $Al_6Ti_2O_{13}$, and $Al_{16}Ti_5O_{34}$ has been realized through various *in situ* techniques and *ab initio* DFT calculations. The results show that the crystallization and co-formation of Al_2TiO_5, $Al_6Ti_2O_{13}$, and $Al_{16}Ti_5O_{34}$ are induced by the migrations of oxygen and its corresponding vacancies. Calculated antisite exchange defect energies by DFT are low, implicating a high degree of cationic mixing for these phases. Similarly, relatively low energy barriers for oxygen migration are found for Al_2TiO_5, whose results also indicate that oxygen vacancies are more prone to exist in the vicinity of Al^{3+} ions than Ti^{4+}. The possible migration of oxygen, combined with HAXPES measurements showing only changes to the O 1s and valence band after annealing, suggests that crystallization of the coatings occurs through a displacive (diffusionless) mechanism. Coherently, these findings emphasize oxygen's significant role and involvement in the phase formation and crystallization of these titanate phases.

ASSOCIATED CONTENT

Supporting Information

The Supporting Information is available free of charge at https://pubs.acs.org/doi/10.1021/acs.jpcc.2c08570.

EBS spectra; ToF-ERDA, HAXPES core-level spectra; and HAXPES survey scan and diffractograms (PDF)

AUTHOR INFORMATION

Corresponding Author

Mats Boman − *Department of Chemistry, Inorganic Chemistry, Ångström Laboratory, Uppsala University, Uppsala SE-75121, Sweden*; Email: Mats.Boman@kemi.uu.se

Authors

Sebastian Öhman − *Department of Chemistry, Inorganic Chemistry, Ångström Laboratory, Uppsala University, Uppsala SE-75121, Sweden*; orcid.org/0000-0002-7071-3917

Axel Forslund − *Department of Materials Science and Engineering, Unit of Structures, KTH Royal Institute of Technology, Stockholm SE-10044, Sweden*

Rebecka Lindblad − *Department of Physics and Astronomy, X-ray Photon Science, Uppsala University, Uppsala SE-75120, Sweden*; orcid.org/0000-0001-6162-1167

Gyula Nagy − *Department of Physics and Astronomy, Applied Nuclear Physics, Ångström Laboratory, Uppsala University, Uppsala SE-75120, Sweden*; orcid.org/0000-0003-3172-5736

Peter Broqvist − *Department of Chemistry, Structural Chemistry, Ångström Laboratory, Uppsala University, Uppsala SE-75121, Sweden*; orcid.org/0000-0002-9842-4332

Elin Berggren − *Department of Physics and Astronomy, X-ray Photon Science, Uppsala University, Uppsala SE-75120, Sweden*; orcid.org/0000-0001-8693-0492

Fredrik O. L. Johansson − *Department of Chemistry, Division of Applied Physical Chemistry, KTH Royal Institute of Technology, Stockholm SE-10044, Sweden; Sorbonne Université, CNRS, Institut des NanoSciences de Paris, INSP, F-75005 Paris, France*; orcid.org/0000-0002-6471-1093

Tobias Törndahl − *Department of Materials Science and Engineering, Solar Cell Technology, Ångström Laboratory, Uppsala University, Uppsala SE-75103, Sweden*; orcid.org/0000-0001-7757-5847

Daniel Primetzhofer − *Department of Physics and Astronomy, Applied Nuclear Physics, Ångström Laboratory, Uppsala University, Uppsala SE-75120, Sweden*; orcid.org/0000-0002-5815-3742

Complete contact information is available at: https://pubs.acs.org/10.1021/acs.jpcc.2c08570

https://doi.org/10.1021/acs.jpcc.2c08570
J. Phys. Chem. C 2023, 127, 6456−6465

Author Contributions

S.Ö.: conceptualization, syntheses, formal analyses HAXPES, visualization, and writing of the original draft. A.F.: DFT calculations of cation antisite defect exchange energies. R.L.: formal analyses HAXPES, writing, and editing. G.N.: RBS and ion beam spectroscopic measurements, writing, and editing. P.B.: DFT calculations of oxygen migration in Al_2TiO_5, writing, and editing. E.B.: formal analyses HAXPES, review, and editing. F.J.: formal analyses HAXPES, review, and editing. T.T.: supervision, review, and editing. D.P.: funding acquisition, supervision, and guidance of ion beam analysis measurements. M.B.: funding acquisition, project administration, and supervision.

Notes

The authors declare no competing financial interest.

■ ACKNOWLEDGMENTS

The Swedish Foundation for Strategic Research (SSF), contract RMA15-0048, along with support from VR-RFI (2019-00191) and SSF (#2019-00191) for accelerator operation at Uppsala University, is greatly acknowledged. For DFT calculations, the Swedish e-science program eESSENCE is also greatly acknowledged. The simulations were performed on resources provided by the Swedish National Infrastructure for Computing (SNIC) at HPC2N and PDC. F.O.L.J acknowledges support from the Swedish Research Council (grant VR 2020-06409). Furthermore, the authors acknowledge SOLEIL for providing synchrotron radiation facilities for HAXPES measurements, and especially thank James Ablett for technical assistance at the beamline "Galaxies". Lastly, the authors thank Katalin Böőr for the beamtime proposal submission and support during the experiments.

■ REFERENCES

(1) Martinolich, A. J.; Kurzman, J. A.; Neilson, J. R. Circumventing Diffusion in Kinetically Controlled Solid-State Metathesis Reactions. *J. Am. Chem. Soc.* **2016**, *138*, 11031−11037.
(2) Noh, M.; Johnson, C. D.; Hornbostel, M. D.; Thiel, J.; Johnson, D. C. Control of Reaction Pathway and the Nanostructure of Final Products through the Design of Modulated Elemental Reactants. *Chem. Mater.* **1996**, *8*, 1625−1635.
(3) Fu, Y.; Wu, T.; Wang, J.; Zhai, J.; Shearer, M. J.; Zhao, Y.; Hamers, R. J.; Kan, E.; Deng, K.; Zhu, X.-Y.; Jin, S. Stabilization of the Metastable Lead Iodide Perovskite Phase via Surface Functionalization. *Nano Lett.* **2017**, *17*, 4405−4414.
(4) Sun, W.; Dacek, S. T.; Ong, S. P.; Hautier, G.; Jain, A.; Richards, W. D.; Gamst, A. C.; Persson, K. A.; Ceder, G. The Thermodynamic Scale of Inorganic Crystalline Metastability. *Sci. Adv.* **2016**, *2*, No. e1600225.
(5) Esposito, V.; Castelli, I. E. Metastability at Defective Metal Oxide Interfaces and Nanoconfined Structures. *Adv. Mater. Interfaces* **2020**, *7*, No. 1902090.
(6) Harada, J. K.; Charles, N.; Poeppelmeier, K. R.; Rondinelli, J. M. Heteroanionic Materials by Design: Progress Toward Targeted Properties. *Adv. Mater.* **2019**, *31*, No. 1805295.
(7) Triana, C. A.; Araujo, C. M.; Ahuja, R.; Niklasson, G. A.; Edvinsson, T. Disentangling the Intricate Atomic Short-Range Order and Electronic Properties in Amorphous Transition Metal Oxides. *Sci. Rep.* **2017**, *7*, No. 2044.
(8) Park, S.; Peddigari, M.; Kim, J. H.; Kim, E.; Hwang, G. T.; Kim, J. W.; Ahn, C. W.; Choi, J. J.; Hahn, B. D.; Choi, J. H.; et al. Selective Phase Control of Dopant-Free Potassium Sodium Niobate Perovskites in Solution. *Inorg. Chem.* **2020**, *59*, 3042−3052.
(9) Martinolich, A. J.; Kurzman, J. A.; Neilson, J. R. Polymorph Selectivity of Superconducting CuSe2 Through Kinetic Control of Solid-State Metathesis. *J. Am. Chem. Soc.* **2015**, *137*, 3827−3833.
(10) Martinolich, A. J.; Neilson, J. R. Toward Reaction-by-Design: Achieving Kinetic Control of Solid State Chemistry with Metathesis. *Chem. Mater.* **2017**, *29*, 479−489.
(11) Todd, P. K.; Neilson, J. R. Selective Formation of Yttrium Manganese Oxides through Kinetically Competent Assisted Metathesis Reactions. *J. Am. Chem. Soc.* **2019**, *141*, 1191−1195.
(12) Kattner, U. R.; Campbell, C. E. Invited Review: Modelling of Thermodynamics and Diffusion in Multicomponent Systems. *Mater. Sci. Technol.* **2009**, *25*, 443−459.
(13) Chen, B.-R.; Sun, W.; Kitchaev, D. A.; Mangum, J. S.; Thampy, V.; Garten, L. M.; Ginley, D. S.; Gorman, B. P.; Stone, K. H.; Ceder, G.; et al. Understanding Crystallization Pathways Leading to Manganese Oxide Polymorph Formation. *Nat. Commun.* **2018**, *9*, No. 2553.
(14) Aykol, M.; Montoya, J. H.; Hummelshøj, J. Rational Solid-State Synthesis Routes for Inorganic Materials. *J. Am. Chem. Soc.* **2021**, *143*, 9244−9259.
(15) Sutter-Fella, C. M. The Value of Watching How Materials Grow: A Multimodal Case Study on Halide Perovskites. *Adv. Energy Mater.* **2021**, *11*, No. 2003534.
(16) Novet, T.; Johnson, D. C. New Synthetic Approach to Extended Solids: Selective Synthesis of Iron Silicides via the Amorphous State. *J. Am. Chem. Soc.* **1991**, *113*, 3398−3403.
(17) Fister, L.; Johnson, D. C.; Brown, R. Synthesis of Copper-Molybdenum-Selenium (CuxMo6Se8) without Binary Compounds as Intermediates: A Study Using Superlattices to Kinetically Control a Solid-State Reaction. *J. Am. Chem. Soc.* **1994**, *116*, 629−633.
(18) Breu, J.; Seidl, W.; Huttner, D.; Kraus, F. Nucleation-Controlled Crystallization of a New, Spontaneously Resolved Solvate of [Ru(Bpy)3](PF6)2 and Its Desolvation Reaction. *Chem. - Eur. J.* **2002**, *8*, 4454−4460.
(19) Stranski, I. N.; Totomanow, D. Keimbildungsgeschwindigkeit Und Ostwaldsche Stufenregel. *Z. Phys. Chem.* **1933**, *163A*, 399−408.
(20) Walser, R. M.; Bené, R. W. First Phase Nucleation in Silicon−Transition-metal Planar Interfaces. *Appl. Phys. Lett.* **1976**, *28*, 624−625.
(21) Öhman, S.; Qiu, R.; Edvinsson, T.; Bäcke, O.; Törndahl, T.; Boman, M. Selective Kinetic Growth and Role of Local Coordination in Forming Al2TiO5-Based Coatings at Lower Temperatures. *Mater. Adv.* **2021**, *2*, 5737−5751.
(22) Barboux, P.; Griesmar, P.; Ribot, F.; Mazerolles, L. Homogeneity-Related Problems in Solution Derived Powders. *J. Solid State Chem.* **1995**, *117*, 343−350.
(23) Öhman, S.; Ek, G.; Nagy, G.; Törndahl, T.; Primetzhofer, D.; Boman, M. Circumventing Thermodynamic Constraints in Nucleation-Controlled Crystallization of Al2TiO5-Based Chemical Vapor Deposition Coatings. *Chem. Mater.* **2022**, *34*, 5151−5164.
(24) Skala, R. D.; Li, D.; Low, I. M. Diffraction, Structure and Phase Stability Studies on Aluminium Titanate. *J. Eur. Ceram. Soc.* **2009**, *29*, 67−75.
(25) Morosin, B.; Lynch, R. W. Structure Studies on Al2TiO5 at Room Temperature and at 600 °C. *Acta Crystallogr., Sect. B: Struct. Crystallogr. Cryst. Chem.* **1972**, *28*, 1040−1046.
(26) Kim, I. J.; Supkwak, H. Thermal Shock Resistance and Thermal Expansion Behaviour With Composition and Microstructure of Al2TiO5 Ceramics. *Can. Metall. Q.* **2000**, *39*, 387−396.
(27) Soofi, M.; Binz, L.; Anderson, W. M. Protective Coating Composition For Molten Aluminium and Alkali Metal Environments. U.S. Patent US10233335B2, 2019.
(28) Tian, S.; Sun, K.; Cui, H.; Xie, X.; Wang, X.; Wei, N.; Wang, H.; Wang, W.; Song, X.; Yang, K. Structural Evolution and Electrochemical Corrosion Behavior of Al−Ti−O Amorphous-Nanocrystalline Composite Films Deposited by Magnetron Sputtering. *Thin Solid Films* **2019**, *692*, No. 137640.
(29) Kim, H. C.; Lee, K. S.; Kweon, O. S.; Aneziris, C. G.; Kim, I. J. Crack Healing, Reopening and Thermal Expansion Behavior of

Al_2TiO_5 Ceramics at High Temperature. *J. Eur. Ceram. Soc.* **2007**, *27*, 1431−1434.
(30) Low, I.-M.; Oo, Z. In Situ Diffraction Study of Self-Recovery in Aluminum Titanate. *J. Am. Ceram. Soc.* **2008**, *91*, 1027−1029.
(31) Kim, I. J. Thermal Stability of Al_2TiO_5 Ceramics for New Diesel Particulate Filter Applications-a Literature Review. *J. Ceram. Process. Res.* **2009**, *10*, 411−418.
(32) Hoffmann, S.; Norberg, S. T.; Yoshimura, M. Structural Models for Intergrowth Structures in the Phase System Al_2O_3−TiO_2. *J. Solid State Chem.* **2005**, *178*, 2897−2906.
(33) Hoffmann, S.; Norberg, S. T.; Yoshimura, M. Melt Synthesis of Al_2TiO_5 Containing Composites and Reinvestigation of the Phase Diagram Al_2O_3−TiO_2 by Powder X-Ray Diffraction. *J. Electroceram.* **2006**, *16*, 327−330.
(34) Norberg, S. T.; Ishizawa, N.; Hoffmann, S.; Yoshimura, M. Redetermination of β-Al_2TiO_5 Obtained by Melt Casting. *Acta Crystallogr., Sect. E: Struct. Rep. Online* **2005**, *61*, i160−i162.
(35) Norberg, S. T.; Hoffmann, S.; Yoshimura, M.; Ishizawa, N. $Al_6Ti_2O_{13}$, a New Phase in the Al_2O_3−TiO_2 System. *Acta Crystallogr., Sect. C: Cryst. Struct. Commun.* **2005**, *61*, i35−i38.
(36) Mehta, N.; Kumar, A. Some New Observations on Activation Energy of Crystal Growth for Thermally Activated Crystallization. *J. Phys. Chem. B* **2016**, *120*, 1175−1182.
(37) Park, Y.; Kim, W.; Kang, Y. Phase Equilibria of Al_2O_3−TiO_x System under Various Oxygen Partial Pressure: Emphasis on Stability of Al_2TiO_5−Ti_3O_5 Pseudobrookite Solid Solution. *J. Eur. Ceram. Soc.* **2021**, *41*, 7362−7374.
(38) Low, I. M.; Lawrence, D.; Smith, R. I. Factors Controlling the Thermal Stability of Aluminum Titanate Ceramics in Vacuum. *J. Am. Ceram. Soc.* **2005**, *88*, 2957−2961.
(39) Papitha, R.; Suresh, M. B.; Chakravarty, D.; Swarnakar, A.; Das, D.; Johnson, R. Eutectoid Decomposition of Aluminum Titanate (Al_2TiO_5) Ceramics under Spark Plasma (SPS) and Conventional (CRH) Thermal Treatments. *Ceram. Int.* **2014**, *40*, 659−666.
(40) Buscaglia, V.; Nanni, P. Decomposition of Al_2TiO_5 and $Al_{2(1-x)}Mg_xTi_{(1+x)}O_5$ Ceramics. *J. Am. Ceram. Soc.* **2005**, *81*, 2645−2653.
(41) Seifert, H. J.; Aldinger, F. Applied Phase Studies / Angewandte Konstitution. *Int. J. Mater. Res.* **1996**, *87*, 841−853.
(42) Violini, M. A.; Hernández, M. F.; Gass, S. E.; Tomba Martinez, A. G.; Rendtorff, N. M. High Temperature Mechanical Behavior of Low Stiffness Al_2TiO_5 and Al_2TiO_5−$3Al_2O_3.2SiO_2$−$ZrTiO_4$ Composite Materials. *Int. J. Appl. Ceram. Technol.* **2022**, *19*, 514−522.
(43) Mayer, M. *SIMNRA User's Guide, Tech. Rep. IPP 9/113*; Max-Planck-Institut für Plasmaphysik: Garching, 1997.
(44) Ström, P.; Primetzhofer, D. Ion Beam Tools for Nondestructive In-Situ and in-Operando Composition Analysis and Modification of Materials at the Tandem Laboratory in Uppsala. *J. Instrum.* **2022**, *17*, No. P04011.
(45) Blöchl, P. E. Projector Augmented-Wave Method. *Phys. Rev. B* **1994**, *50*, 17953−17979.
(46) Kresse, G.; Hafner, J. Ab Initio Molecular Dynamics for Liquid Metals. *Phys. Rev. B* **1993**, *47*, 558−561.
(47) Kresse, G.; Hafner, J. Ab Initio Molecular-Dynamics Simulation of the Liquid-Metal–Amorphous-Semiconductor Transition in Germanium. *Phys. Rev. B* **1994**, *49*, 14251−14269.
(48) Kresse, G.; Furthmüller, J. Efficient Iterative Schemes for Ab Initio Total-Energy Calculations Using a Plane-Wave Basis Set. *Phys. Rev. B* **1996**, *54*, 11169−11186.
(49) Kresse, G.; Furthmüller, J. Efficiency of Ab-Initio Total Energy Calculations for Metals and Semiconductors Using a Plane-Wave Basis Set. *Comput. Mater. Sci.* **1996**, *6*, 15−50.
(50) Perdew, J. P.; Burke, K.; Ernzerhof, M. Generalized Gradient Approximation Made Simple. *Phys. Rev. Lett.* **1996**, *77*, 3865−3868.
(51) Monkhorst, H. J.; Pack, J. D. Special Points for Brillouin-Zone Integrations. *Phys. Rev. B* **1976**, *13*, 5188−5192.
(52) Methfessel, M.; Paxton, A. T. High-Precision Sampling for Brillouin-Zone Integration in Metals. *Phys. Rev. B* **1989**, *40*, 3616−3621.
(53) Jonsson, H.; Millis, G.; Jacobsen, K. W. In *Classical and Quantum Dynamics in Condensed Phase Simulations*, Proceedings of the International School of Physics, LERICI, Villa Marigola; Berne, B. J.; Cicotti, G.; Coker, D. F., Eds.; World Scientific, 1998; p 880.
(54) Larsen, A. H.; Mortensen, J. J.; Blomqvist, J.; Castelli, I. E.; Christensen, R.; Dułak, M.; Friis, J.; Groves, M. N.; Hammer, B.; Hargus, C.; et al. The Atomic Simulation Environment-a Python Library for Working with Atoms. *J. Phys. Condens. Matter* **2017**, *29*, No. 273002.
(55) Lodesani, F.; Tavanti, F.; Menziani, M. C.; Maeda, K.; Takato, Y.; Urata, S.; Pedone, A. Exploring the Crystallization Path of Lithium Disilicate through Metadynamics Simulations. *Phys. Rev. Mater.* **2021**, *5*, No. 075602.
(56) Karthika, S.; Radhakrishnan, T. K.; Kalaichelvi, P. A Review of Classical and Nonclassical Nucleation Theories. *Cryst. Growth Des.* **2016**, *16*, 6663−6681.
(57) Oyelaran, O.; Novet, T.; Johnson, C. D.; Johnson, D. C. Controlling Solid-State Reaction Pathways: Composition Dependence in the Nucleation Energy of InSe. *J. Am. Chem. Soc.* **1996**, *118*, 2422−2426.
(58) Jiang, H.; Tseng, J.; Neuber, N.; Barrirero, J.; Adam, B.; Frey, M.; Dippel, A.; Banerjee, S.; Gallino, I.; Feng, A.; et al. On the Devitrification of Cu−Zr−Al Alloys: Solving the Apparent Contradiction between Polymorphic Liquid-Liquid Transition and Phase Separation. *Acta Mater.* **2022**, *226*, No. 117668.
(59) Thieme, K.; Avramov, I.; Rüssel, C. The Mechanism of Deceleration of Nucleation and Crystal Growth by the Small Addition of Transition Metals to Lithium Disilicate Glasses. *Sci. Rep.* **2016**, *6*, No. 25451.
(60) Blázquez, J. S.; Conde, C. F.; Conde, A. Kinetics of Nanocrystallization in FeCoNbB (Cu) Alloys. *Appl. Phys. A: Mater. Sci. Process.* **2003**, *76*, 571−575.
(61) Kantre, K.; Moro, M. V.; Moldarev, D.; Johansson, D.; Wessman, D.; Wolff, M.; Primetzhofer, D. SIGMA: A Set-up for In-Situ Growth, Material Modification and Analysis by Ion Beams. *Nucl. Instrum. Methods Phys. Res., Sect. B* **2020**, *463*, 96−100.
(62) Leavitt, J. A.; McIntyre, L. C.; Ashbaugh, M. D.; Oder, J. G.; Lin, Z.; Dezfouly-Arjomandy, B. Cross Sections for 170.5° Backscattering of ^4He from Oxygen for ^4He Energies between 1.8 and 5.0 MeV. *Nucl. Instrum. Methods Phys. Res., Sect. B* **1990**, *44*, 260−265.
(63) Zhu, Q.; Peng, Y.; Lin, L.; Fan, C.-M.; Gao, G.-Q.; Wang, R.-X.; Xu, A.-W. Stable Blue TiO_{2-x} Nanoparticles for Efficient Visible Light Photocatalysts. *J. Mater. Chem. A* **2014**, *2*, 4429−4437.
(64) Wang, W.; Lu, C.-H.; Ni, Y.-R.; Song, J.-B.; Su, M.-X.; Xu, Z.-Z. Enhanced Visible-Light Photoactivity of {001} Facets Dominated TiO_2 Nanosheets with Even Distributed Bulk Oxygen Vacancy and Ti^{3+}. *Catal. Commun.* **2012**, *22*, 19−23.
(65) Khan, H.; Swati, I. K. Fe^{3+}-Doped Anatase TiO_2 with d−d Transition, Oxygen Vacancies and Ti^{3+} Centers: Synthesis, Characterization, UV−Vis Photocatalytic and Mechanistic Studies. *Ind. Eng. Chem. Res.* **2016**, *55*, 6619−6633.
(66) Zheng, J.; Liu, Y.; Ji, G.; Zhang, P.; Cao, X.; Wang, B.; Zhang, C.; Zhou, X.; Zhu, Y.; Shi, D. Hydrogenated Oxygen-Deficient Blue Anatase as Anode for High-Performance Lithium Batteries. *ACS Appl. Mater. Interfaces* **2015**, *7*, 23431−23438.
(67) Innocenzi, P.; Martucci, A.; Armelao, L.; Licoccia, S.; Di Vona, M. L.; Traversa, E. Sol-Gel Synthesis of β-Al_2TiO_5 Thin Films at Low Temperature. *Chem. Mater.* **2000**, *12*, 517−524.
(68) Siol, S.; Mann, J.; Newman, J.; Miyayama, T.; Watanabe, K.; Schmutz, P.; Cancellieri, C.; Jeurgens, L. P. H. Concepts for Chemical State Analysis at Constant Probing Depth by Lab-Based XPS/HAXPES Combining Soft and Hard X-Ray Sources. *Surf. Interface Anal.* **2020**, *52*, 802−810.
(69) Céolin, D.; Ablett, J. M.; Prieur, D.; Moreno, T.; Rueff, J.-P.; Marchenko, T.; Journel, L.; Guillemin, R.; Pilette, B.; Marin, T.; et al. Hard X-Ray Photoelectron Spectroscopy on the GALAXIES Beamline at the SOLEIL Synchrotron. *J. Electron Spectrosc. Relat. Phenom.* **2013**, *190*, 188−192.

(70) Rueff, J.-P.; Ablett, J. M.; Céolin, D.; Prieur, D.; Moreno, T.; Balédent, V.; Lassalle-Kaiser, B.; Rault, J. E.; Simon, M.; Shukla, A. The GALAXIES Beamline at the SOLEIL Synchrotron: Inelastic X-Ray Scattering and Photoelectron Spectroscopy in the Hard X-Ray Range. *J. Synchrotron Radiat.* **2015**, *22*, 175−179.
(71) Moulder, J. F.; Stickle, W. F.; Sobol, P. E.; Bomben, K. D. *Handbook of X-Ray Photoelectron Spectroscopy: A Reference Book of Standard Spectra for Identification and Interpretation of XPS Data*; Chastain, J., Ed.; Perkin-Elmer Corporation: Minnesota, 1992.
(72) Biesinger, M. C.; Lau, L. W. M.; Gerson, A. R.; Smart, R. S. C. Resolving Surface Chemical States in XPS Analysis of First Row Transition Metals, Oxides and Hydroxides: Sc, Ti, V, Cu and Zn. *Appl. Surf. Sci.* **2010**, *257*, 887−898.
(73) Biesinger, M. C.; Payne, B. P.; Hart, B. R.; Grosvenor, A. P.; McIntryre, N. S.; Lau, L. W. M.; Smart, R. S. Quantitative Chemical State XPS Analysis of First Row Transition Metals, Oxides and Hydroxides. *J. Phys.: Conf. Ser.* **2008**, *100*, No. 012025.
(74) Ilatovskaia, M.; Savinykh, G.; Fabrichnaya, O. Thermodynamic Description of the Ti-Al-O System Based on Experimental Data. *J. Phase Equilib. Diffus.* **2017**, *38*, 175−184.
(75) Paul-Boncour, V.; Lindbaum, A.; Latroche, M.; Heathman, S. Homogeneity Range and Order−Disorder Transitions in R1−xNi2 Laves Phase Compounds. *Intermetallics* **2006**, *14*, 483−490.
(76) Joubert, J.-M.; Černý, R.; Latroche, M.; Leroy, E.; Guénée, L.; Percheron-Guégan, A.; Yvon, K. A Structural Study of the Homogeneity Domain of LaNi5. *J. Solid State Chem.* **2002**, *166*, 1−6.
(77) Rau, H. Range of Homogeneity and Defect Energetics in Co1−x S. *J. Phys. Chem. Solids* **1976**, *37*, 931−934.
(78) Sizov, F. F.; Plyatsko, S. V. Homogeneity Range and Nonstoichiometric Defects in IV−VI Narrow-Gap Semiconductors. *J. Cryst. Growth* **1988**, *92*, 571−580.
(79) Rempel, A. A.; Gusev, A. I. Preparation of Disordered and Ordered Highly Nonstoichiometric Carbides and Evaluation of Their Homogeneity. *Phys. Solid State* **2000**, *42*, 1280−1286.
(80) Kim, Y.-M.; He, J.; Biegalski, M. D.; Ambaye, H.; Lauter, V.; Christen, H. M.; Pantelides, S. T.; Pennycook, S. J.; Kalinin, S. V.; Borisevich, A. Y. Probing Oxygen Vacancy Concentration and Homogeneity in Solid-Oxide Fuel-Cell Cathode Materials on the Subunit-Cell Level. *Nat. Mater.* **2012**, *11*, 888−894.
(81) Adler, S. B. Chemical Expansivity of Electrochemical Ceramics. *J. Am. Ceram. Soc.* **2004**, *84*, 2117−2119.
(82) Aidhy, D. S.; Lu, C.; Jin, K.; Bei, H.; Zhang, Y.; Wang, L.; Weber, W. J. Formation and Growth of Stacking Fault Tetrahedra in Ni via Vacancy Aggregation Mechanism. *Scr. Mater.* **2016**, *114*, 137−141.
(83) Dey, U.; Chatterjee, S.; Taraphder, A. Antisite-Disorder Engineering in La-Based Oxide Heterostructures via Oxygen Vacancy Control. *Phys. Chem. Chem. Phys.* **2018**, *20*, 17871−17880.
(84) Ruban, A. V. Single-Site Mean-Field Approach to Thermal Defects in Binary Ordered Alloys. *Philos. Mag.* **2014**, *6435*, 1192−1201.
(85) Epicier, T.; Thomas, G.; Wohlfromm, H.; Moya, J. S. High Resolution Electron Microscopy Study of the Cationic Disorder in Al2TiO5. *J. Mater. Res.* **1991**, *6*, 138−145.
(86) Ohya, Y.; Kawauchi, Y.; Ban, T. Cation Distribution of Pseudobrookite-Type Titanates and Their Phase Stability. *J. Ceram. Soc. Japan* **2017**, *125*, 695−700.
(87) Grimes, R. W.; Pilling, J. Defect Formation in β-Al2TiO5 and Its Influence on Structure Stability. *J. Mater. Sci.* **1994**, *29*, 2245−2249.

https://doi.org/10.1021/acs.jpcc.2c08570
J. Phys. Chem. C 2023, 127, 6456−6465